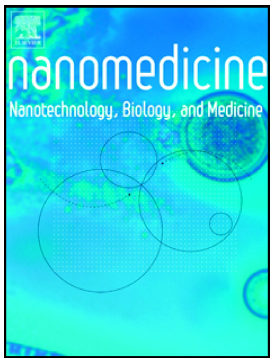

New prospects in skin regeneration and repair using nanophased hydroxyapatite embedded in collagen nanofibers

Nilza Ribeiro, Aureliana Sousa, Cassilda Cunha-Reis, Ana Leite Oliveira, Pedro L. Granja, Fernando J. Monteiro, Susana R. Sousa

PII: S1549-9634(20)30207-0

DOI: https://doi.org/10.1016/j.nano.2020.102353

Reference: NANO 102353

To appear in: *Nanomedicine: Nanotechnology, Biology, and Medicine*

Revised date: 16 December 2020

Please cite this article as: N. Ribeiro, A. Sousa, C. Cunha-Reis, et al., New prospects in skin regeneration and repair using nanophased hydroxyapatite embedded in collagen nanofibers, *Nanomedicine: Nanotechnology, Biology, and Medicine* (2021), https://doi.org/10.1016/j.nano.2020.102353

New prospects in skin regeneration and repair using nanophased hydroxyapatite embedded in collagen nanofibers

Nilza Ribeiro[1,2,3*], Aureliana Sousa[1,2*], Cassilda Cunha-Reis[4], Ana Leite Oliveira[4], Pedro L. Granja[1,2#], Fernando J. Monteiro[1,2,3#], Susana R. Sousa[1,2,5#]

[1]i3S - Instituto de Investigação e Inovação em Saúde, Universidade do Porto, Rua Alfredo Allen, 208, 4200-135 Porto, Portugal

[2]INEB - Instituto de Engenharia Biomédica, Porto, Rua Alfredo Allen, 208, 4200-135 Porto, Portugal

[3]FEUP – DEMM, Faculdade de Engenharia, da Universidade do Porto, Rua Roberto Frias, 4200-465 Porto, Portugal

[4]Universidade Católica Portuguesa, CBQF - Centro de Biotecnologia e Química Fina – Laboratório Associado, Escola Superior de Biotecnologia, Porto, Portugal

[5]ISEP – Instituto Superior de Engenharia do Porto, Politécnico do Porto, Rua Dr. António Bernardino de Almeida, 431, 4200-072 Porto, Portugal

*These authors contributed equally to this work

#Joint senior authors

Corresponding author:

Susana R Sousa

ssousa@ineb.up.pt

word count of body text: 4471+ 497=4968 words

number of references: 60

number of figures: 7

Abstract: 147

KEY WORDS

Composite biomaterial, skin wound healing, Collagen electrospinning, Hydroxyapatite electrospraying and Calcium ions

ABSTRACT

This study reflects an exploitation of a composite matrix produced by electrospinning of collagen and electrospraying of nanophased hydroxyapatite (nanoHA), for skin regeneration applications. The main goal was to evaluate the effect of nanoHA, as source of localized calcium delivery, on human dermal fibroblasts, keratinocytes, and human mesenchymal stem cells (hMSCs) growth, proliferation, differentiation, and extracellular matrix production. This study revealed that calcium ions provided by nanoHA significantly enhanced cellular growth and proliferation rates and prevented adhesion of pathogenic bacteria strains typically found in human skin flora. Moreover, hMSCs were able to differentiate in both osteogenic and adipogenic lineages. Rat subcutaneous implantation of the membranes also revealed that no adverse reaction occurred. Therefore, the mechanically fit composite membrane presents a great potential to be used either as cell transplantation scaffold for skin wound regeneration or as wound dressing material in plastic surgery, burns treatment or skin diseases.

1.Introduction

Recently, several strategies in skin bioengineering have been investigated in order to overcome the limitations of the conventional therapeutic approaches, such as autografts or allografts, applied in the patients suffering from skin lesions (chronic/diabetic ulcers, burns, and pressure wounds).[1-4] Autografts are limited in their extent, inducing scarring, lengthy hospital stays, while allografts present ethical and safety issues related with disease transmission, and may lead to immune rejection, highlighting the demand for effective substitutes. The ideal bioengineered skin substitute should be easily handled, readily transplanted, non-immunogenic, able to induce the rapid formation of vascularized skin adhering to the wound bed and avoiding scarring.[5] Furthermore, in burns treatment there is a need to prevent infection while promoting the reconstruction of several layers of tissue, such as dermis and hypodermis near bone tissue.

The most common cell types employed on skin substitutes are allogeneic fibroblasts (dermal component) and keratinocytes (epidermal layer), although adipose-derived stem cells are already used in latest studies. Mesenchymal cells can differentiate into bone or skin cells according to the surrounding microenvironment constitution[7]. Due to their easy production, high proliferative potential, pluripotency and lack of ethical constraints human mesenchymal stem cells (hMSCs) represent also a promising cell source, overcoming senescence related problems reported with the use of differentiated cell lines[7-9]. Furthermore, the local application of hMSCs derived from human umbilical cord blood successfully improved skin-substitute wound healing[10, 11]. It has also been demonstrated that paracrine factors from hMSCs recruit macrophages and endothelial lineage cells and enhance wound healing, possibly due to decreasing of inflammation levels[12].

The production of electrospun nanofibers based on biocompatible polymers for the regeneration of several tissues has been explored in recent years, due to their capacity to mimic the hierarchical structure of the natural extracellular matrices[13-19]. Their highly porous structure and spatial interconnectivity is a characteristic which is known to be essential to the nutrient and waste transport and cell communication, thus supporting cellular phenomena such as adhesion,

differentiation and proliferation, making electrospun nanofibers well-suited as wound dressing material[20, 21]. To produce these electrospun nanofibers materials ranging from natural to synthetic polymers have been engineered: collagen[22-25], chitosan[26], PCL, PVA and polyacrylonitrile[27], polyethersulfone[28] poly-e-caprolactone/collagen nanofibers[29], collagen-hydroxyapatite[30], PLGA/collagen[31] and chitosan/PVA[32] among others. Besides biodegradability and biocompatibility, these materials can be chemically modified and functionalized with growth factors or proteins to promote cell response, thus improving the signaling cascade inherent to processes of wound healing and skin regeneration[14]. It has been described that calcium ions play an important role in the regeneration of connective tissue and repair of skin[33, 34], activation of metalloproteinases[35], as well as, keratinocyte growth and differentiation[36].

This work aims to study the suitability of a previously developed biocomposite[37] based on collagen electrospun nanofibers embedded with hydroxyapatite crystals for applications in skin Tissue Engineering. The effect of nanoHA on the overall performance of this biocomposite was evaluated with special emphasis, since a combined collagen/nanoHA biomaterial applied for *in vitro*/*in vivo* experimentation regarding skin repair is uncommon in the literature. As nanoHA was nonsintered, it may act as a source of localized calcium delivery into biocomposite microenvironment.

The ability of biocomposite to accommodate growth and proper function of several cell types (primary fibroblasts, keratinocytes and hMSCs) that are central in skin regeneration was assessed. Microbiological tests were also conducted using bacterial strains found in human skin flora. The collagen/nanoHA newly developed membranes with 90 μm thickness, revealed to be self-sustained, easily manipulated and stretchable, thus revealing high potential for use as a wound dressing with excellent tensile and mechanical proprieties. The promising results obtained is this study suggests a successful application of this collagen/nanoHA biocomposite for skin regeneration and repair, seeking to fill the gap on literature concerning this thematic.

2.Methods

2.1 Biomaterials development

The innovative membranes used in this study derive from a prototype previously described [37]. Briefly, both prototype and membranes were designed using an approach that combines electrospinning of collagen type I and electrospraying of nanoHA onto 10 mm diameter coverglasses or directly onto aluminum foil wrapped on a rotating cylinder collector over 1 h and 8 hours, respectively, using collagen non-denaturing conditions and non-toxic reagents. The coverglasses coated with electrospun collagen fibers plus nanoHA were used in all *in vitro* assays, while the membranes obtained after 8h of co- electrospinning/electrospraying and after detaching from the aluminum foil were used in the *in vivo* study. The substrates were chemically cross-linked using a solution of 20 mM 1-ethyl-3 [3-(dimethylamino)propyl] carbodiimide hydrochloride and 10 mM N-hydroxysulfosuccinimide sodium salt. Prior to each *in vitro* or *in vivo* experiment, the scaffolds were sterilized by immersion in a series of dilute ethanol solutions of 90, 70 and 50% (v/v).

2.2 Calcium release

The calcium release from collagen/nanoHA samples was assessed by Inductively Coupled Plasma-Atomic Emission Spectroscopy (ICP-AES). Collagen/HA substrates were incubated with 0.9% (v/v) NaCl solution at 37°C and 5% CO_2 in a humidified chamber. After 1, 7, 14 and 21 days of incubation, 500µL of incubation medium were withdrawn and replaced by fresh 0.9% NaCl solution. All tests were performed in duplicate.

2.3 *S. aureus* and *S. epidermidis* cultures

The distribution, morphology, as well as the number of adherent *Staphylococcus aureus* (*S. aureus*) ATCC 25923 strain and *S. epidermidis* RP62A strain bacteria cultured on biocomposite surfaces were studied. Nutrient agar plate inoculated with the respective bacteria strain was incubated at 37°C for 18h. Bacterial suspensions with $1.5x10^8$ colony-forming units (CFU)/mL were prepared using a densitometer (BioMerieux). To allow bacterial adhesion onto biomaterial surfaces, 1mL of bacterial suspension was placed on each sample and incubated in a gently shaking water bath at 37°C for 2h. The experiment was performed in triplicate. After the incubation period, substrates were washed twice with NaCl to remove non-adherent bacteria,

transferred to tubes containing 5 mL of NaCl and sonicated for 1 second at 20kHz using a sonicator (Sonoplus HD 2200, Bandelin) with a MS73 probe. Sonicated solutions were used to make serial dilutions, and these were placed onto nutrient agar culture plates and incubated at 37°C for 18h. Afterwards, the number of adherent bacteria was counted, and the number of CFU/mL was calculated. Coverglasses coated with Poly-D-lysine hydrobromide (PDL) were used as control.

2.4 Cell culture

Pooled Human Dermal Neonatal Fibroblasts (HDNF) (Corriel Institute), HaCaT keratinocytes and hMSCs (Lonza, USA) were cultured in DMEM with 10% FBS and 1% P/S at 37°C and 5% CO_2 in a humidified chamber. Cells were seeded on the biocomposite samples at a cell seeding density of $5x10^3$ cells/mL in case of HDNF and hMSCs and $1x10^4$ cells/mL in case of HaCaT. Coverglasses coated with PDL were used as control. At defined time points (1, 7, 14 and 21 days) samples were collected and processed for subsequent analysis of cell metabolic activity, adhesion, morphology, proliferation, differentiation, and ECM deposition.

2.5 Scanning electron microscopy (SEM)

For SEM observations, cell-seeded samples were fixed with 1.5% (v/v) glutaraldehyde, dehydrated with an increasing ethanol–water gradient and dried using hexamethyldisilazane. SEM analyses used a FEI Quanta 400FEG/EDAX Genesis X4M (Hillsboro, OR USA) scanning electron microscope under high vacuum conditions. Samples were palladium–gold coated, using a sputter coater (SPI-Module) in an argon atmosphere before imaging. The elemental composition of collagen/nanoHA electrospun samples, visualized by SEM as described above was performed using X-ray microanalysis and electron backscattered diffraction analysis.

2.6 Cell metabolic activity

To assess metabolic activity six samples from each independent experiment were used.

Briefly, 20% (v/v) resazurin solution was added ono each well. After 3h at 37°C fluorescence was read using λex=530 nm and λem=590 nm in a microplate reader (Biotek, Synergy MX,

USA). The fluorescence value corresponding to the non-seeded substrates was subsequently subtracted.

2.7 Immunocytochemistry

For immunostaining, the cell-seeded surfaces were fixed with 4wt% paraformaldehyde and permeabilized with 0.1% (v/v) triton X-100 and incubated in 1wt% BSA for 30 min at room temperature (RT). ECM components were visualized by using rabbit anti-fibronectin (f3648, 1:400), rabbit anti-laminin and mouse anti-collagen IV. Simultaneously with secondary antibody incubation, the samples were incubated with the conjugated probe phalloidin/Alexa Fluor® 488 (1:40) for F-actin staining. Cell nuclei were counterstained with 4',6-diamidino-2-phenylindole (Vectashield/DAPI) dye, immediately before confocal visualization confocal laser scanning microscopy (CLSM, Leica SP2AOBS) using LCS software (Leica Microsystems). The scanned Z-series were projected onto a single plane (Z-projection) using ImageJ. Final figure panels were composed using Adobe Photoshop (Adobe Systems, USA).

2.8 Cell proliferation

After cell staining (section 2.7), the proliferation marker Ki67 (anti-rabbit) was used at the time of DAPI analysis allowing the visualization of cell's nucleus. Automated High-throughput sample analysis was then carried out. Image acquisition was done in the INCell 2000 Analyzer (GE Healthcare) with a 10x objective. Quantification of Ki67 positive/negative cells was done using the Developer Toolbox software (GE Healthcare) and visual data inspection was performed with SpotfireDecisionSite®.

2.9 Fibroblast/keratinocyte co-culture model

HNDFs were cultured for 10 days on the top of PDL coated coverglasses (control), collagen electrospun membranes and collagen/nanoHA biocomposites (initial seeding density of $2.5x10^3$ cells/sample). Following this period, HaCaT keratinocytes were seeded on top of the fibroblast monolayer. After 7 days from keratinocyte seeding the samples were sent for SEM analysis as specified in section 2.6.

2.10 Osteogenic and Adipogenic differentiation of hMSCs

For osteogenic differentiation, $15x10^3$ hMSCs were seeded on top of each sample (PDL and collagen/nanoHA matrices), allowed to grow for 7 days and cultured for further 21 days under basal or osteogenic induction conditions (total time in culture 28 days). The basal medium for osteogenic differentiation (BMo) consisted in DMEM-glutamax/low glucose with 10% (v/v) FBS and 1% (v/v) P/S. Osteogenic medium consisted of BMo supplemented with $5x10^5$ M ascorbic acid, 0.1 μM dexamethasone and 0.01 M β-glycerophosphate. Media was exchanged twice a week.

For adipogenic diferentiation, $6x10^3$ hMSCs were seeded on top of each sample and allowed to reach a monolayer for a week in basal medium (BMa), consisted in DMEM-glutamax/low glucose, 10% (v/v) of FBS and 1% (v/v) P/S. Scheduled media exchanges were performed either with adipogenic medium (AM) (BMa supplemented with 10^{-4}M dexamethasone, $5x10^{-4}$M IBMX, insulin 10 μg/mL and 10^{-4}M indomethacin) or insulin media (IM) (BMa with 10 μg/mL of insulin), according to the following scheme: AM on days 1,6 and 11 and IM on days 4,9 and 14. After day 14 cells in adipogenic differentiation were maintained on IM for 1 week (day 21), changing the media once.

2.11Alkaline phosphatase/oil red O staining and colorimetric assays

Samples from osteogenic differentiation experiments were analyzed to perform alkaline phosphatase (ALP) activity evaluation. Briefly, samples were fixed with PFA 4% (v/v) in HBSS (1X) for 20 min at RT followed by incubation in a Fast Violet B salt solution (0.25 mg/mL) containing 4% (v/v) of naphthol AS-MX phosphate alkaline solution (0.25wt%) for 45 min at RT.

For adipogenic differentiation evaluation, oil red O staining was performed. Firstly, samples were incubated in a solution of 60% (v/v) isopropanol for 5 min and then in an oil red solution for 5 min. Hematoxylin was used as a counterstain and observed under a stereomicroscope (Olympus SZX2-ILLT, Olympus, Japan) coupled with a camera (DP21 Olympus) using the EPview software for image acquisition.

2.12 Mechanical tests

The mechanical properties of the nanofiber mats were assessed by uniaxial tensile testing using a texture analyzer (TA. XT.Plus®, Stable Micro Systems, UK), based on ASTM D882-02 methods. These matrices were cut into rectangular strips of 0.75cmx3cm and maintained immersed in PBS for 6 h at RT prior to testing. After hydration equilibrium was reached, sample thickness was measured with a digital micrometer (MI20, AdamelLhomargy, France) with the average thickness of 6 samples being 92±32 µm. Then, the samples were mounted on the grips and the tests were carried out at a crosshead speed of 5 mm/min. Young's modulus, tensile strength, elongation at break and strain energy were calculated from the obtained stress/strain curves. The results represent the average of six samples.

2.13 *In vivo* study

Collagen/nanoHA mats were produced as described in section 2.1 and cut into 1cm^2 sections. All animal experiments were carried out following protocols approved by the Ethics Committee competent regulatory national authorities. Rats were housed at 22ºC with a 12h light/dark cycle and had ad libitum access to water and food. Male rats (Wistar, 9 weeks old, 250-300g, 5 animals) were used as recipients. The animals were anesthetized by ketamine/xylazine (80 and 10 mg/Kg respectively) and anesthesia was maintained over the course of surgery by continuous isofluorane delivery. The dorsal surgical sites were shaved and sterilized. Two subcutaneous pockets were created per rat for sample insertion. After implantation, incisions were closed with sutures and analgesics were administrated (4 mg tramadol HCl/kg). The animals were routinely monitored for general appearance, activity, and healing of the implant sites, and were euthanized after one week for retrieval of implants. No rats were lost during the study.

2.14 Histological evaluation

The harvested samples, which included the entire sample and some surrounding tissue, were fixed in 10% (v/v) neutral-buffered formalin overnight and processed for paraffin embedding. Using standard incubation conditions, samples were sectioned onto slides (4mm) and stained with standard protocols for Masson's trichrome and Hematoxylin-Eosin staining.

2.15 Statistical analysis

Statistical analysis for metabolic activity data was assessed using non-parametric one-way ANOVA. Bonferroni correction was used in all statistical tests with multiple groups. P-values were considered statistically significant when bellow 0.05.

3.Results

ICP-AES analysis revealed that the amount of calcium released from collagen nanofibers/nanoHA biocomposite after an incubation period of 1 day in 0.9% NaCl solution was approximately 0.33% of the total amount of calcium present in each sample (**Fig. 1C**). For the other established timepoints (7, 14 and 21 days), the calcium contained in the respective supernatant solutions was considerably inferior to day 1, indicating that the calcium release was not gradual but immediate in an initial burst release event (**Fig. 1C**). Most calcium ions remained inside the non-sintered HA crystals and thus these may easily provide localized calcium ions for subsequent interactions with molecules, cells, or bacteria. Corroborating the prior results, the X-rays energy dispersive spectra (**Fig. S1** in supporting information) of hydroxyapatite (Z1), coverglass surface (Z2) and collagen (Z3) confirm that the nanoHA agglomerates stayed inside 3D-like structure between the collagen mesh, (calcium and phosphorous peaks in Z1) (**Fig. S1, B**). It was previously shown that these matrices were produced using non-denaturing conditions, therefore the native conformation of collagen was preserved after electrospinning procedure. The fabrication process did not impact the integrity of collagen's triple helix on this nanostructured collagen-nanoHA composite, nor did the inclusion of nanoHA. In fact, this ratio for denatured collagen is around 0.5, while for intact collagen is around 1, and the composites presented a ratio of 1.07[37].

Electrospun nanofiber membranes display excellent porosity with high interpore-connectivity, particularly important to allow the transfer of exudate from the wounded area. Also, the small pore size and high specific surface area enable the nanofiber membranes to inhibit the invasion of exogenous microorganisms to the wound site [38] lowering the potential for infection.

Microbiological tests were developed to assess the adherence and proliferation of two bacterial strains normally present in human skin flora. In healthy individuals both *S. epidermidis* and *S. aureus* are maintained at levels non-toxic levels to the host, however upon skin injury, these can enter the injury site inducing infection [39]. According to *S. epidermidis* adhesion levels, the total number of CFU/mL was statistically significantly lower for collagen/nanoHA surfaces than for control samples representing a total of 20% decrease (**Fig.1A** and **1B**). In terms of morphology, the two bacteria strains tested presented their normal spherical shape (coccus), yet a distinct bacterial distribution depending on the material type (**Fig.1A**). Adhesion to control surfaces followed the typical form of bacterial aggregates, while the biocomposite surfaces showed isolated bacteria. Calcium ions are known to decrease bacterial adhesion [7], leading to the hypothesis that the nanoHA present in the composite matrices was in fact hindering bacterial proliferation.

Cell seeding efficiency of fibroblast (HDNF) cultures on PDL coated coverglasses, collagen matrices and collagen/nanoHA composite matrices was obtained by comparing the initial number of cells seeded per sample and DAPI signal quantification after 1day; on PDL samples the rate of seeding efficiency was 38±4%, a percentage above the one obtained for the collagen samples (26±5%) but very similar to that of collagen/nanoHA matrices (42±4%).

The pattern of metabolic activity in all substrates tested increased with incubation time, as expected, highlighting the significant higher values found in the composite scaffolds for the longest culture times (**Fig.2B**). At day 7, HDNF cultured on both control and collagen samples presented typical elongated fibroblast shape and cell guidance in their distribution, unlike the composite surfaces where HDNFs appeared more spread and randomly distributed (**Fig. 2A**). After 14 days, a compact film of cells was formed on the various substrates. During the acquisition of CLSM images related to HDNF adhesion on biocomposite surfaces, the number of sections required to cover all layers of cells (z axis distance) was much higher (260μm) when compared to control samples (160μm), indicating that the composite network structures induced

the formation of a higher number of cell layers, which is in agreement with the metabolic activity data.

Proliferation rates were quantified only for 1 and 7 days after cell seeding (**Fig.2C**, image), since samples from later timepoints had excessive numbers of cells, making it technically impossible to quantify the total cell number by DAPI. Also, the signals emitted by the Ki67 antibody that marks cells that are undergoing a proliferative state, were impossible to obtain at days 14 and 21, because the antibody solution could not reach the cell's nuclei, due to the highly intricate ECM meshes already deposited by the HDNF. The number of proliferating cells was 19%, 10% and 15%, 1-day post seeding, for PDL, collagen and collagen/nanoHA composite samples, respectively (**Fig.2C**, graph). These proliferation rates resembled those determined for standard 2D culture on TCPS culture flasks (approximately 20%). As expected, the proliferation rates decreased significantly with the incubation period as the increasing number of cells reduced the available space. Notably for day 7 of culture, the proliferation rate for composite samples (6%) was considerably higher than the rate found in PDL samples (2%).

The deposition of expressed ECM proteins normally produced by dermal fibroblasts such as collagen IV, fibronectin (data not shown) and laminin, was confirmed in low levels by day 7 post-seeding, progressively increased over the following 14 days, with the most prominent expression seen at day 21 (**Fig.3**). An increase in ECM protein deposition over time was particularly obvious in the case of the collagen/nanoHA composite.

The collagen/nanoHA biomaterial allowed adhesion and growth of keratinocytes (epidermal cells) with a seeding efficient and metabolic activity identical to collagen substrates, establishing a confluent monolayer by day 7 post-seeding, proving that these cells were able to proliferate (**Fig.4A and B**).

As proof-of-concept, it was decided to establish a co-culture model of fibroblasts and keratinocytes. In **Figure4C,** a compact film of cells may be observed, making almost impossible to distinguish keratinocytes from fibroblasts. The analysis of cellular metabolic

activity suggests that there has been an increase with time of culture, without significant differences between the different materials (**Fig. 4D**).

The hMSCs behaved similarly to the fibroblasts, they were able to attach, proliferate and occupy the entire surface of the samples over the 21 days of culture (**Fig.5A**).

The cytoskeletal architecture visualization by labelling f-Actin after 24h of initial seeding showed that the adhesion via focal contact seemed to be more significant on the collagen/nanoHA matrices in comparison to the control materials (**Fig.5B**). After longer culture timepoints the main difference is seen in terms of cell orientation. While on PDL and collagen samples cells seem to be organized in layers parallel to one another, perpendicularly aligned cell layers stacked on top of each other are observed on collagen/nanoHA matrices.

The hMSCs cultured on control samples revealed a significantly higher metabolic activity compared to collagen and collagen/nanoHA materials for the initial culture timepoints. After 14 days, hMSCs cultured on collagen nanofibers with and without nanoHA recovered this difference, displaying RFU values similar to the control (**Fig.5C**). In accordance with metabolic activity results, the filling of the various tested surfaces was identical for the later incubation timepoints (**Fig.S2** in supporting information). Regarding osteogenic differentiation, PDL and collagen/nanoHA samples were kept in both basal and osteoinductive media and differentiation evaluation was assessed in terms of ALP activity. Under basal conditions, there was no evidence of ALP activity, since no ALP staining (red) was detected for any timepoint. This indicates that osteogenic differentiation did not occur in the 21 days period when no differentiation stimuli were provided, suggesting that collagen/nanoHA matrices were not performing as an osteoinductive environment *per se*. When the culture medium was supplemented with osteoinductive factors, ALP staining could be observed both in control and collagen/nanoHA samples showing that hMSCs differentiated and matured into osteogenic lineage. ALP staining appeared to be even stronger on collagen/nanoHA mats when compared to PDL samples (**Fig.6A**). Regarding adipogenic differentiation, all samples cultured in adipogenic medium, and stained with Oil red after 21 days, revealed fat vacuoles in the cells

(**Fig.6B**). This clearly indicated that collagen/nanoHA matrices were able to support hMSCs viability and differentiation without pre-committing these stromal cells into any specific lineage.

Envisaging a skin tissue engineering application, the collagen/nanoHA membrane (**Fig.7a'**) was produced according to the 8h process described in section 2.1, in order to provide easily implantable materials for *in vivo* biological assessment. The tensile properties of these developed composite membranes with an average thickness of 90µm, were evaluated through mechanical tests (**Fig.7A**). The stiffness of the composite materials was given by the Young's Modulus (8,46±1,05 kPa). The tensile strength of the same material was 428±54 kPa, whereas the elongation at break and strain energy were 174±16%, 11,4±3,5 MJ/m^3, respectively.

A preliminary study was performed to understand how these mechanical suitable collagen/nanoHA matrices interact *in vivo*. The implantation of the composite matrices was performed by creating two subcutaneous pockets inside the dorsum of 6 male Wistar rats. All animals did not show any complication throughout the entire implantation time. After one week, rats were euthanized, and the autopsy of the implantation site revealed modifications in the morphology of the composite matrices. After 7 days implanted, matrices were very easy to visualize macroscopically upon retrieval (**Fig.7b'**, black arrow). Histological analysis of the implantation site showed that the biomaterial maintained its structural integrity and elicited only a mild physiological reaction (**Fig.7C-D**). Mononuclear cells were present at the surfaces of the implanted meshes, and some of these cells penetrated the surface structure of the biomaterial (**Fig.7c''**). There was no consistent vascularization of the matrix structure, however, a few blood vessels could be seen within the sample structure (**Fig.7c''**, black arrows).

4.Discussion

Collagen based matrices have long been used to enhance fibroblastic adhesion [40] mainly because collagen family of proteins is a major constituent of dermal ECM [41]. Many approaches to achieve adhesiveness and bioactivity of biomaterials are based on coating them with ECM

molecules, such as fibronectin, vitronectin, laminin, and collagen[42]. Laminins, are the most bioactive components in basement membranes where they assemble into a cross-linked network, interwoven with the type IV collagen network[43]. Currently, collagen nanofibrous scaffolds are the most developed biomimetic skin substitute due to their biological origin, low antigenicity and nanotopography.[44] Electrospun collagen favors cell attachment, growth and proliferation and decreases wound contraction when compared to freeze-dried collagen scaffolds.[23] In the present study using electrospun collagen/nanoHA matrices inspired on the native ECM nanofibrillar structure[37], it was possible to obtain high levels of initial cell adhesion sites for all the tested cell types, while maintaining the ability of HNDF, keratinocytes and hMSCs to proliferate on these scaffolds. In addition, HNDFs were able to produce and deposit laminin, fibronectin, and collagen IV, which ultimately allows and supports the stacking of multiple cell layers.

The infections caused by gram-positive bacteria present in the skin flora (*S. epidermidis*/*S. aureus*) are often associated with surgeries, hospital stay, dialysis, catheters, percutaneous and intravascular medical devices, prosthetic joints and large wounds.[45] The interactions between bacteria and the host ECM proteins allow the early colonization of tissues and biomaterials through their ability to produce biofilms. [46] The resistance to bacterial adhesion and growth ability associated to hydroxyapatite has been studied as a potential way to prevent bacterial colonization, contamination and infection.[47, 48] According to the microbiological results obtained in this work, adhesion of *S. epidermidis* to the collagen/nanoHA biocomposite was expected, as already reported[49], although significantly lower compared to the control samples and surprisingly different from the typical cluster shaped distribution.

Another reason to consider these scaffolds as promising candidates for skin regeneration is the availability of calcium ions from HA that remained in the nanostructured biocomposite network for long periods, as evidenced by the low calcium levels released. Therefore these ions may act synergistically with others agents like polydeoxyribonucleotides or L-carnitine, promoting skin repair and regeneration.[22] An early study indicated that hydroxyapatite can have a mitogenic

effect on cultured mammalian cells[50] thus, increasing proliferation rates. In another work, fibronectin-functionalized HA coatings significantly promoted dermal fibroblast attachment *in vitro*, by measuring the number of focal adhesions per unit cell area[51]. Synthetic HA coatings and topographic surface modifications have been included to enhance the skin-implant seal and plasma-sprayed HA coatings were also applied to transcutaneous devices with 0.7mm pores to enhance dermal fibroblastic attachment *in vivo* by over 10%[52, 53] . Our findings revealed that calcium ions provided by HA enhanced significantly cellular growth and proliferation of both skin differentiated cells (fibroblasts and keratinocytes) and hMSCs.

Collagen/nanoHA biocomposite holds a composition very similar to bone, but the present study showed that it can also be applied in soft tissues such as skin. The presence of HA did not induce the differentiation of stem cells onto the osteogenic lineage, in fact it was proved that hMSCs can be differentiated into adipocytes. This happens as opposed to what had been reported in studies of similar biomaterials where human adipose derived stem cells differentiated into mature osteoblasts even in the absence of specific inducing factors[54].

An adequate mechanical performance of skin tissue is fundamental to its healthy functionality. Effort has been put towards understanding the biomechanical properties of skin, and the literature shows that the reported values of key parameters such as ultimate tensile strength, Young's modulus, elongation at break and strain energy vary greatly according to age[55], body location, orientation with respect to Langer´s lines, test type and testing conditions [56]. The developed collagen/nanoHA composite displayed remarkable tensile properties. The observed linear elastic deformation denotes good elastic recoil until break, mimicking natural skin deformation under low stress [57]. Elongation at break and strain energy are comparable to those of human skin and skin substitutes[56, 58], evidencing that this material possesses adequate elasticity and toughness for skin regeneration applications. The stiffness of the collagen/nanoHA mats was within the range of values previously reported from *in vivo* measurements on forearm skin[59]. Tensile strength however was one order of magnitude lower than what has been described for skin[56] but comparable to that of collagen nanofiber mats

proposed for skin regeneration[60]. A preliminary pilot study on the *in vivo* subcutaneous implantation of these mechanically stable matrices was performed and no adverse reaction occurred from the host organism was detected, as well as no encapsulation of the membranes was detected although early indication of *de novo* vascularization was observed. The mechanically fit composite membranes presented an excellent rate of cell colonization and bacteriostatic properties fundamental in preventing infections and may therefore be potential candidates for skin repair or act as functionalized membranes for guided skin regeneration.

ACKNOWLEGEMENTS

The authors would like to acknowledge the financial support from Fundação para a Ciência e a Tecnologia, Portugal, for N. Ribeiro's PhD grant (SFRH/BD/69686/2010) and A. Sousa position (UID/BIM/04293/2013/POCI-01-0145-FEDER-007274). Also, the provision of nanoHA (nanoXIM) by FLUIDINOVA, S.A. (Portugal) and collagen by Kensey Nash (USA) is greatly acknowledged. The authors are thankful to Maria Pia Ferraz (UFP) for her support with the microbiology facilities. The authors acknowledge the support of the i3S Scientific Platforms "Bioimaging" and "BioSciences Screening", members of the national infrastructure Portuguese Platform of Bioimaging (PPBI-POCI-01-0145-FEDER-022122).

References

1. Hodgkinson T, Bayat A. Dermal substitute-assisted healing: Enhancing stem cell therapy with novel biomaterial design. *Arch Dermatol Res* 2011,**303**:301-15.

2. Low ZWK, Li ZB, Owh C, Chee PL, Ye EY, Dan K, et al. Recent innovations in artificial skin. *Biomater Sci* 2020,**8**:776-97.

3. Van Der Veen VC, Boekema BKHL, Ulrich MMW, Middelkoop E. New dermal substitutes. *Wound Repair and Regeneration* 2011,**19**:s59-s65.

4. Yu JR, Navarro J, Coburn JC, Mahadik B, Molnar J, Holmes DH, et al. Current and future perspectives on skin tissue engineering: Key features of biomedical research, translational assessment, and clinical application. *Advanced Healthcare Materials* 2019,**8**:19.

5. Brusselaers N, Monstrey S, Vogelaers D, Hoste E, Blot S. Severe burn injury in europe: A systematic review of the incidence, etiology, morbidity, and mortality. *Crit Care* 2010,**14**:12.

6. Bottcher-Haberzeth S, Biedermann T, Reichmann E. Tissue engineering of skin. *Burns* 2010,**36**:450-60.

7. Jin GR, Prabhakaran MP, Ramakrishna S. Stem cell differentiation to epidermal lineages on electrospun nanofibrous substrates for skin tissue engineering. *Acta Biomater* 2011,**7**:3113-22.

8. Han YF, Chai JK, Sun TJ, Li DJ, Tao R. Differentiation of human umbilical cord mesenchymal stem cells into dermal fibroblasts in vitro. *Biochem Biophys Res Commun* 2011,**413**:561-65.

9. Sasaki M, Abe R, Fujita Y, Ando S, Inokuma D, Shimizu H. Mesenchymal stem cells are recruited into wounded skin and contribute to wound repair by transdifferentiation into multiple skin cell type. *J Immunol* 2008,**180**:2581-87.

10. Luo GX, Cheng WG, He WF, Wang XJ, Tan JL, Fitzgerald M, et al. Promotion of cutaneous wound healing by local application of mesenchymal stem cells derived from human umbilical cord blood. *Wound Repair and Regeneration* 2010,**18**:506-13.

11. Nakagawa H, Akita S, Fukui M, Fujii T, Akino K. Human mesenchymal stem cells successfully improve skin-substitute wound healing. *Br J Dermatol* 2005,**153**:29-36.

12. Chen LW, Tredget EE, Wu PYG, Wu YJ. Paracrine factors of mesenchymal stem cells recruit macrophages and endothelial lineage cells and enhance wound healing. *Plos One* 2008,**3**:12.

13. Bhardwaj N, Kundu SC. Electrospinning: A fascinating fiber fabrication technique. *Biotechnol Adv* 2010,**28**:325-47.

14. Kubinova S, Sykova E. Nanotechnologies in regenerative medicine. *Minim Invasive Ther Allied Technol* 2010,**19**:144-56.

15. Liu HF, Ding XL, Zhou G, Li P, Wei X, Fan YB. Electrospinning of nanofibers for tissue engineering applications. *J Nanomater* 2013,**2013**:11.

16. Melchels FPW, Domingos MaN, Klein TJ, Malda J, Bartolo PJ, Hutmacher DW. Additive manufacturing of tissues and organs. *Prog Polym Sci* 2012,**37**:1079-104.

17. Reddy VJ, Radhakrishnan S, Ravichandran R, Mukherjee S, Balamurugan R, Sundarrajan S, et al. Nanofibrous structured biomimetic strategies for skin tissue regeneration. *Wound Repair and Regeneration* 2013,**21**:1-16.

18. Vasita R, Katti DS. Nanofibers and their applications in tissue engineering. *Int J Nanomed* 2006,**1**:15-30.

19. Yang G, Li X, He Y, Ma JK, Ni GL, Zhou SB. From nano to micro to macro: Electrospun hierarchically structured polymeric fibers for biomedical applications. *Prog Polym Sci* 2018,**81**:80-113.

20. Dias JR, Granja PL, Bartolo PJ. Advances in electrospun skin substitutes. *Prog Mater Sci* 2016,**84**:314-34.

21. Kumbar SG, Nair LS, Bhattacharyya S, Laurencin CT. Polymeric nanofibers as novel carriers for the delivery of therapeutic molecules. *J Nanosci Nanotechnol* 2006,**6**:2591-607.

22. Gennero L, De Siena R, Denysenko T, Roos MA, Calisti GF, Martano M, et al. A novel composition for in vitro and in vivo regeneration of skin and connective tissues. *Cell Biochemistry and Function* 2011,**29**:311-33.

23. Powell HM, Supp DM, Boyce ST. Influence of electrospun collagen on wound contraction of engineered skin substitutes. *Biomaterials* 2008,**29**:834-43.

24. Rho KS, Jeong L, Lee G, Seo BM, Park YJ, Hong SD, et al. Electrospinning of collagen nanofibers: Effects on the behavior of normal human keratinocytes and early-stage wound healing. *Biomaterials* 2006,**27**:1452-61.

25. Rnjak-Kovacina J, Wise SG, Li Z, Maitz PKM, Young CJ, Wang Y, et al. Electrospun synthetic human elastin:Collagen composite scaffolds for dermal tissue engineering. *Acta Biomater* 2012,**8**:3714-22.

26. Jayakumar R, Prabaharan M, Nair SV, Tamura H. Novel chitin and chitosan nanofibers in biomedical applications. *Biotechnol Adv* 2010,**28**:142-50.

27. Liu X, Lin T, Fang JA, Yao G, Zhao HQ, Dodson M, et al. In vivo wound healing and antibacterial performances of electrospun nanofibre membranes. *J Biomed Mater Res Part A* 2010,**94A**:499-508.

28. Babaeijandaghi F, Shabani I, Seyedjafari E, Naraghi ZS, Vasei M, Haddadi-Asl V, et al. Accelerated epidermal regeneration and improved dermal reconstruction achieved by polyethersulfone nanofibers. *Tissue Eng Part A* 2010,**16**:3527-36.

29. Choi JS, Lee SJ, Christ GJ, Atala A, Yoo JJ. The influence of electrospun aligned poly(epsilon-caprolactone)/collagen nanofiber meshes on the formation of self-aligned skeletal muscle myotubes. *Biomaterials* 2008,**29**:2899-906.

30. Wahl DA, Czernuszka JT. Collagen-hydroxyapatite composites for hard tissue repair. *Eur Cells Mater* 2006,**11**:43-56.

31. Liu SJ, Kau YC, Chou CY, Chen JK, Wu RC, Yeh WL. Electrospun plga/collagen nanofibrous membrane as early-stage wound dressing. *J Membr Sci* 2010,**355**:53-59.

32. Kang YO, Yoon IS, Lee SY, Kim DD, Lee SJ, Park WH, et al. Chitosan-coated poly(vinyl alcohol) nanofibers for wound dressings. *J Biomed Mater Res Part B* 2010,**92B**:568-76.

33. Kawai K, Larson BJ, Ishise H, Carre AL, Nishimoto S, Longaker M, et al. Calcium-based nanoparticles accelerate skin wound healing. *Plos One* 2011,**6**.

34. Lansdown ABG. Calcium: A potential central regulator in wound healing in the skin. *Wound Repair and Regeneration* 2002,**10**:271-85.

35. Tallant C, Marrero A, Gomis-Ruth FX. Matrix metalloproteinases: Fold and function of their catalytic domains. *Biochim Biophys Acta-Mol Cell Res* 2010,**1803**:20-28.

36. Bikle DD, Xie Z, Tu C-L. Calcium regulation of keratinocyte differentiation. *Expert Review of Endocrinology & Metabolism* 2012,**7**:461-72

37. Ribeiro N, Sousa SR, Van Blitterswijk CA, Moroni L, Monteiro FJ. A biocomposite of collagen nanofibers and nanohydroxyapatite for bone regeneration. *Biofabrication* 2014,**6**.

38. Khil MS, Cha DI, Kim HY, Kim IS, Bhattarai N. Electrospun nanofibrous polyurethane membrane as wound dressing. *J Biomed Mater Res Part B* 2003,**67B**:675-79.

39. Nilsson M, Frykberg L, Flock JI, Pei L, Lindberg M, Guss B. A fibrinogen-binding protein of staphylococcus epidermidis. *Infect Immun* 1998,**66**:2666-73.

40. Balin A, Vilenchik M. Connective tissue. In: Schulz R, Noelker L, Rockwood K, Sprott R, editors. The encyclopedia of aging. 4th ed. New York: Springer; 2016. p. 260–61.

41. Oswald J, Steudel C, Salchert K, Joergensen B, Thiede C, Ehninger G, et al. Gene-expression profiling of cd34+ hematopoietic cells expanded in a collagen i matrix. *STEM CELLS* 2006,**24**:494-500.

42. Shin H, Jo S, Mikos AG. Biomimetic materials for tissue engineering. *Biomaterials* 2003,**24**:4353-64.

43. Von Der Mark K, Park J, Bauer S, Schmuki P. Nanoscale engineering of biomimetic surfaces: Cues from the extracellular matrix. *Cell and Tissue Research* 2009,**339**:131-53.

44. Sundaramurthi D, Krishnan UM, Sethuraman S. Electrospun nanofibers as scaffolds for skin tissue engineering. *Polymer Reviews* 2014,**54**:348-76.

45. Otto M. Staphylococcus epidermidis — the 'accidental' pathogen. *Nature Reviews Microbiology* 2009,**7**:555-67.

46. Gordon RJ, Lowy FD. Pathogenesis of methicillin-resistant staphylococcus aureus infection. *Clinical Infectious Diseases* 2008,**46**:S350-S59.

47. Aronov D, Rosen R, Ron EZ, Rosenman G. Electron-induced surface modification of hydroxyapatite-coated implant. *Surface and Coatings Technology* 2008,**202**:2093-102.

48. Ragab HS, Ibrahim FA, Abdallah F, Al-Ghamdi AA, El-Tantawy F, Radwan N, et al. Synthesis and in vitro antibacterial properties of hydroxyapatite nanoparticles. *IOSR Journal of Pharmacy and Biological Sciences* 2014,**9**:77-85.

49. Barros J, Grenho L, Manuel CM, Ferreira C, Melo L, Nunes OC, et al. Influence of nanohydroxyapatite surface properties on staphylococcus epidermidis biofilm formation. *Journal of Biomaterials Applications* 2014,**28** 1325-35.

50. Cheung HS, Story MT, Mccarty DJ. Mitogenic effects of hydroxyapatite and calcium pyrophosphate dihydrate crystals on cultured mammalian cells. *Arthritis & Rheumatism* 1984,**27**:668-74.

51. J. PC, M. E-H, W. BG. The development of fibronectin-functionalised hydroxyapatite coatings to improve dermal fibroblast attachment in vitro. *The Journal of Bone and Joint Surgery British volume* 2012,**94-B**:564-69.

52. J. PC, D. G, A. MC, Man SSN, W. BG. Sealing the skin barrier around transcutaneous implants. *The Journal of Bone and Joint Surgery British volume* 2008,**90-B**:114-21.

53. Pendegrass CJ, Goodship AE, Blunn GW. Development of a soft tissue seal around bone-anchored transcutaneous amputation prostheses. *Biomaterials* 2006,**27**:4183-91.

54. Calabrese G, Giuffrida R, Fabbi C, Figallo E, Lo Furno D, Gulino R, et al. Collagen-hydroxyapatite scaffolds induce human adipose derived stem cells osteogenic differentiation in vitro. *PLoS One* 2016,**11**:e0151181.

55. Daly CH, Odland GF. Age-related changes in the mechanical properties of human skin. *Journal of Investigative Dermatology* 1979,**73**:84-87.

56. Annaidh AN, Bruyere K, Destrade M, Gilchrist MD, Ottenio M. Characterization of the anisotropic mechanical properties of excised human skin. *Journal of the Mechanical Behavior of Biomedical Materials* 2012,**5**:139-48.

57. Hussain SH, Limthongkul B, Humphreys TR. The biomechanical properties of the skin. *Dermatologic Surgery* 2013,**39**:193-203.

58. Yu B, Kang SY, Akthakul A, Ramadurai N, Pilkenton M, Patel A, et al. An elastic second skin. *Nature Materials* 2016,**15**:911-+.

59. Boyer G, Laquièze L, Le Bot A, Laquièze S, Zahouani H. Dynamic indentation on human skin in vivo: Ageing effects. *Skin Research and Technology* 2009,**15**:55-67.

60. Zhou T, Sui B, Mo X, Sun J. Multifunctional and biomimetic fish collagen/bioactive glass nanofibers: Fabrication, antibacterial activity and inducing skin regeneration in vitro and in vivo. *Int J Nanomedicine* 2017,**12**:3495-507.

Figure legends

Figure 1 - Morphology and distribution analyzed by SEM imaging (A) and total number of CFU/mL (B) of *S. epidermidis* and *S. aureus* seeded on coverglasses coated with PDL (control) and collagen/nanoHA composites. Scale bar:10µm. *Indicates a statistically significant difference from control cultures ($p<0.05$). (C) Calcium cumulative released percentage from collagen/nanoHA composites versus time.

Figure 2 – Morphology and cytoskeletal organization analyzed by SEM and CLSM imaging (A), metabolic activity (B) and proliferation (C) of fibroblasts cultured on coverglasses coated with PDL (control), collagen substrates and collagen/nanoHA composites versus time. In CLSM images f-actin is indicated in green and nuclei in blue, scale bar:100 µm. In SEM images scale

bar:100 µm (50 µm for the higher magnification). *Indicates a statistically significant difference from the control cultures. § indicates a statistically significant difference from the cultures grown on the collagen substrates ($p<0.05$). (C) presents a graph depicting proliferation rates.

Figure 3 – Laminin deposition evaluation followed by CLSM imaging of fibroblasts cultured on coverglasses coated with PDL, collagen substrates and collagen/nanoHA composites over time. F-actin is indicated in green, laminin in red and nuclei in blue. Scale bar:100µm.

Figure 4 - Keratinocyte morphology and cytoskeletal organization followed by CLSM imaging (A) after 7-day seeding on collagen substrates and collagen/nanoHA composites and metabolic activity (B) versus time. Fibroblast/keratinocyte co-culture on coverglasses coated with PDL, collagen substrates and collagen/nanoHA composites analyzed by SEM imaging (C) and metabolic activity (D) versus time. F-actin is indicated in green and nuclei in blue. Scale bar:100µm.

Figure 5 - Morphology and cytoskeletal organization analyzed by SEM (A) and CLSM (B) imaging and metabolic activity (C) of hMSCs cultured on coverglasses coated with PDL (control), collagen substrates and collagen/nanoHA composites versus time. In CLSM images f-actin is indicated in green and nuclei in blue, scale bar:100µm. In SEM images scale bar:100µm (50µm for the higher magnification). *Indicates a statistically significant difference with respect from the control cultures §indicates a statistically significant difference from the cultures grown on the collagen substrates ($p<0.05$).

Figure 6 – hMSC differentiation into osteogenic and adipogenic lineages, after culture on coverglasses coated with PDL and collagen/nanoHA composites. (A) Representative images of hMSCs cultured in basal and osteogenic differentiation medium stained for ALP. (B) Representative images of hMSCs cultured in basal medium and adipogenic differentiation medium. The fat vacuoles are indicated in red. Black scale bars:250µm and white scale bars:100µm.

Figure 7 – *In vivo* implantation of collagen/nanoHA composite membranes. (A) A representative stress-strain plot; (a') macroscopic image of produced composite membrane (scale bar:500μm). (B) Male Wistar after composite membrane implantation; (b') arrow indicates the implanted sample upon retrieval after 7 days. (C) Masson trichrome colorimetric staining of implanted composite; red (keratin and muscle fibers), blue/green (collagen fibers), light red/pink (cytoplasm) and dark brown/black (nuclei). Scale bar:500μm. C′ and c′′ represent higher magnifications (scale bar:100μm). (D) Hematoxylin and eosin staining of implanted composite membrane; light pink (cytoplasm) and purple (nuclei). Scale bar:500μm. D′ and d′′ represent higher magnifications (scale bar:100μm).

Graphical abstract

A mechanically fit composite membrane as wound dressing material based on collagen nanofibers and nanophased hydroxyapatite obtained by simultaneous use of electrospinning and electrospraying, respectivelly. The material presented an excellent rate of cell colonization, support hMSCs differentiation onto adipogenic lineage and bacteriostatic properties fundamental in preventing infections, highlighting the potential of the developed composite in a wide range of skin engineering applications.

Author statement

Nilza Ribeiro, Aureliana Sousa, Cassilda Cunha-Reis, Ana Leite Oliveira, Pedro L. Granja, Fernando J. Monteiro, Susana R. Sousa contributed to the study design, conceptualization and methodology. Nilza Ribeiro and Aureliana Sousa conducted the research and investigation process performing the experimental studies and both drew the schemes and figures, contributing equaly to the manuscript. Cassilda Cunha-Reis and Ana Leite Oliveira were responsible for the mechanical tests and all authors analysed the data and approved the final manuscript wrote by Nilza Ribeiro and Aureliana Sousa.

Highlights

- Calcium ions enhance growth and proliferation of skin differentiated cells and hMSCs
- Adipogenic differentiation of hMSCs over composite network rich in calcium
- Nanostructured composite prevents adhesion of typical human skin pathogenic bacteria
- Mechanically fit composite membrane as wound dressing material

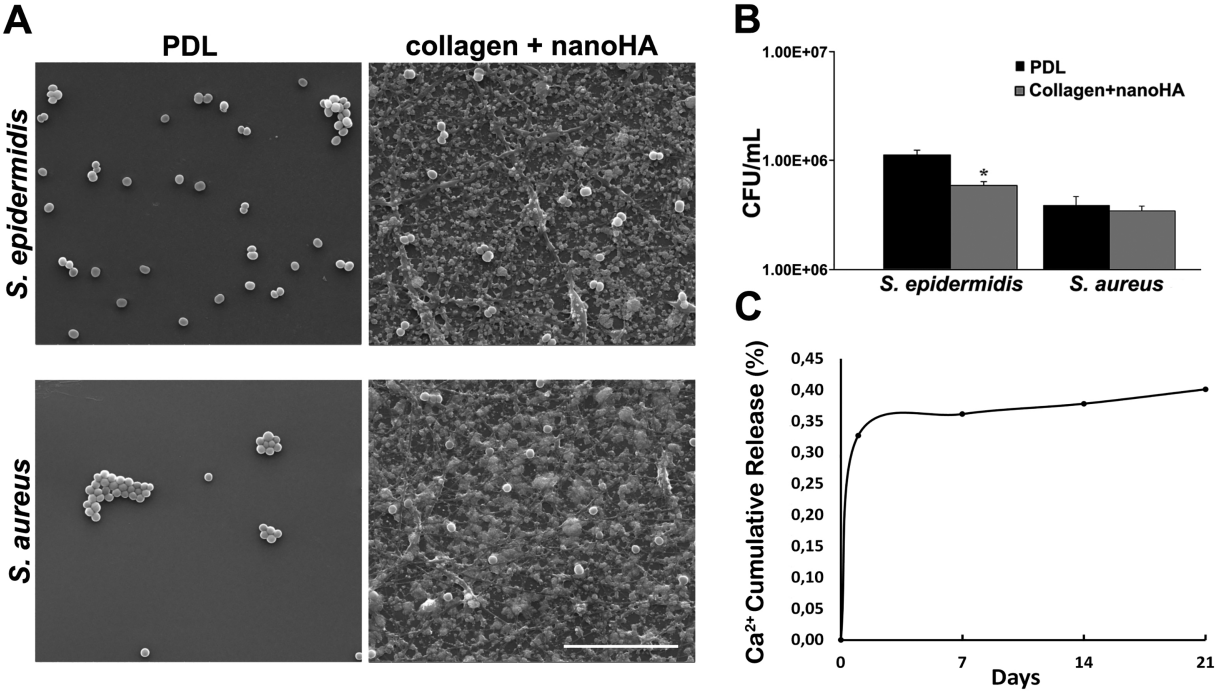
A
PDL
collagen + nanoHA
S. epidermidis
S. aureus
B
1.00E+07
1.00E+06
1.00E+06
CFU/mL
PDL
Collagen+nanoHA
*
S. epidermidis
S. aureus
C
Ca2+ Cumulative Release (%)
0,45
0,40
0,35
0,30
0,25
0,20
0,15
0,10
0,05
0,00
0
7
14
21
Days

Figure 1

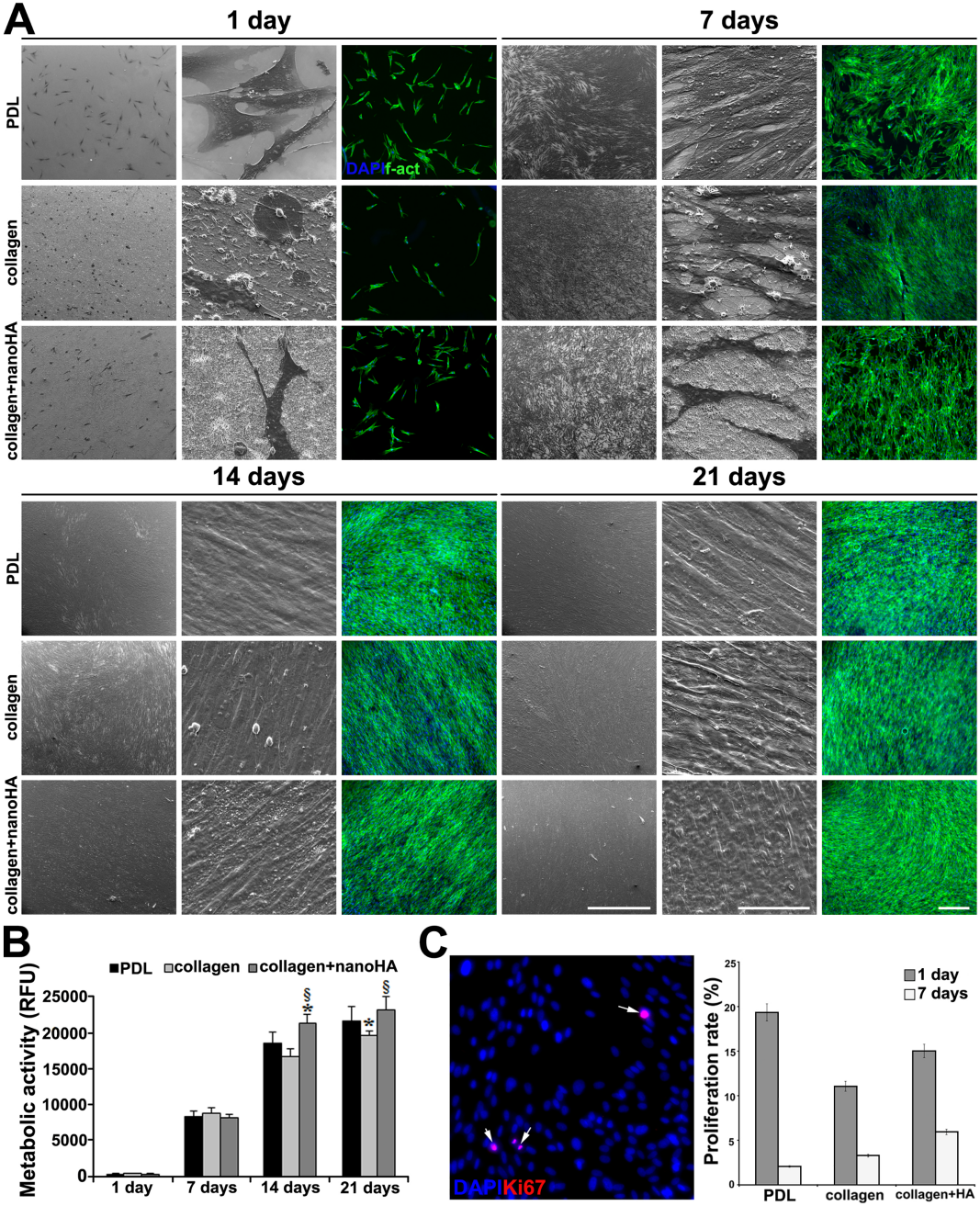
A
1 day
7 days
14 days
21 days
PDL
collagen
collagen+nanoHA
DAPI f-act
B
PDL
collagen
collagen+nanoHA
Metabolic activity (RFU)
25000
20000
15000
10000
5000
0
1 day
7 days
14 days
21 days
§
*
C
DAPI Ki67
Proliferation rate (%)
25
20
15
10
5
0
1 day
7 days
PDL
collagen
collagen+HA

Figure 2

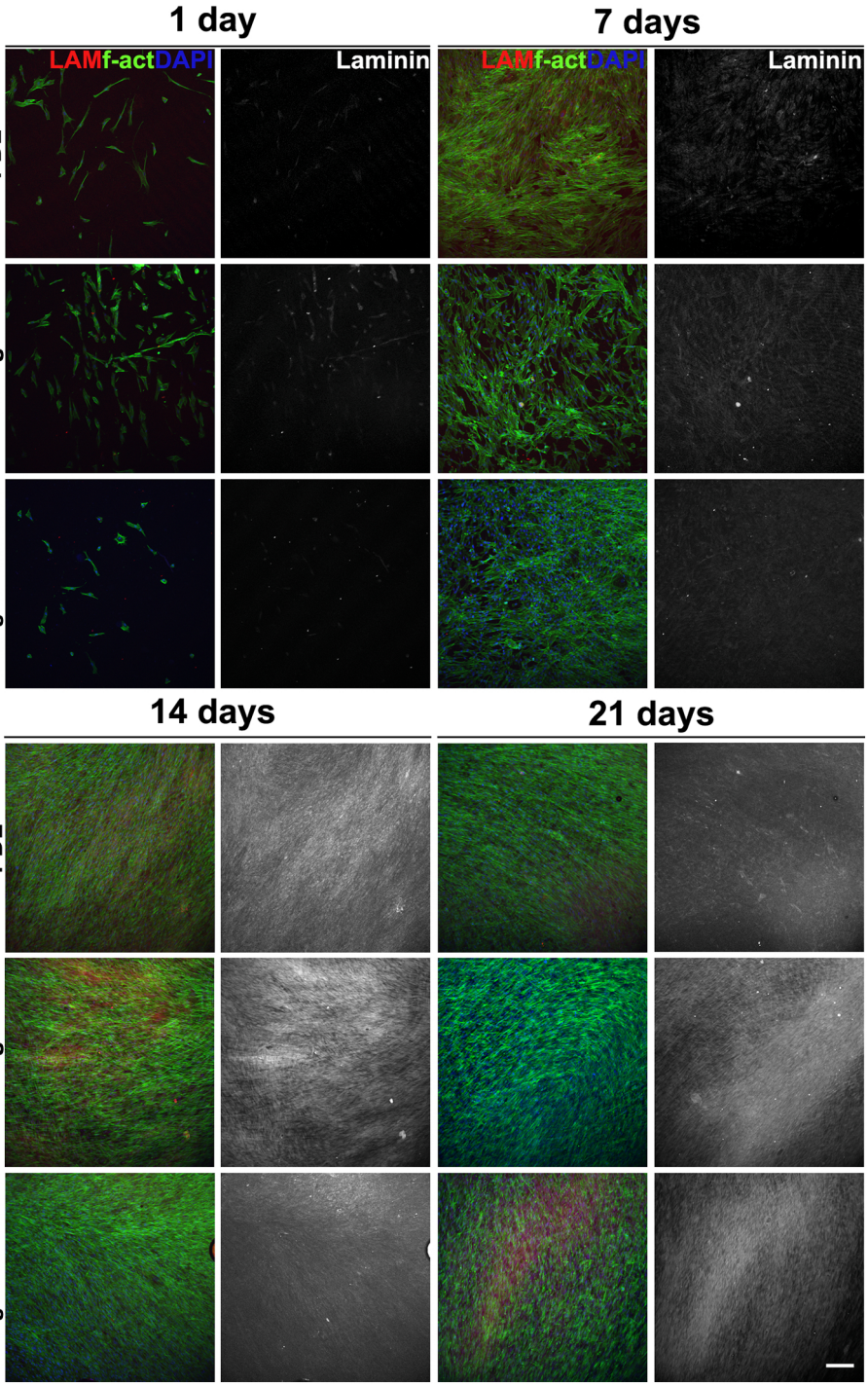
1 day
7 days
LAMf-actDAPI
Laminin
PDL
collagen
collagen+nanoHA
14 days
21 days

Figure 3

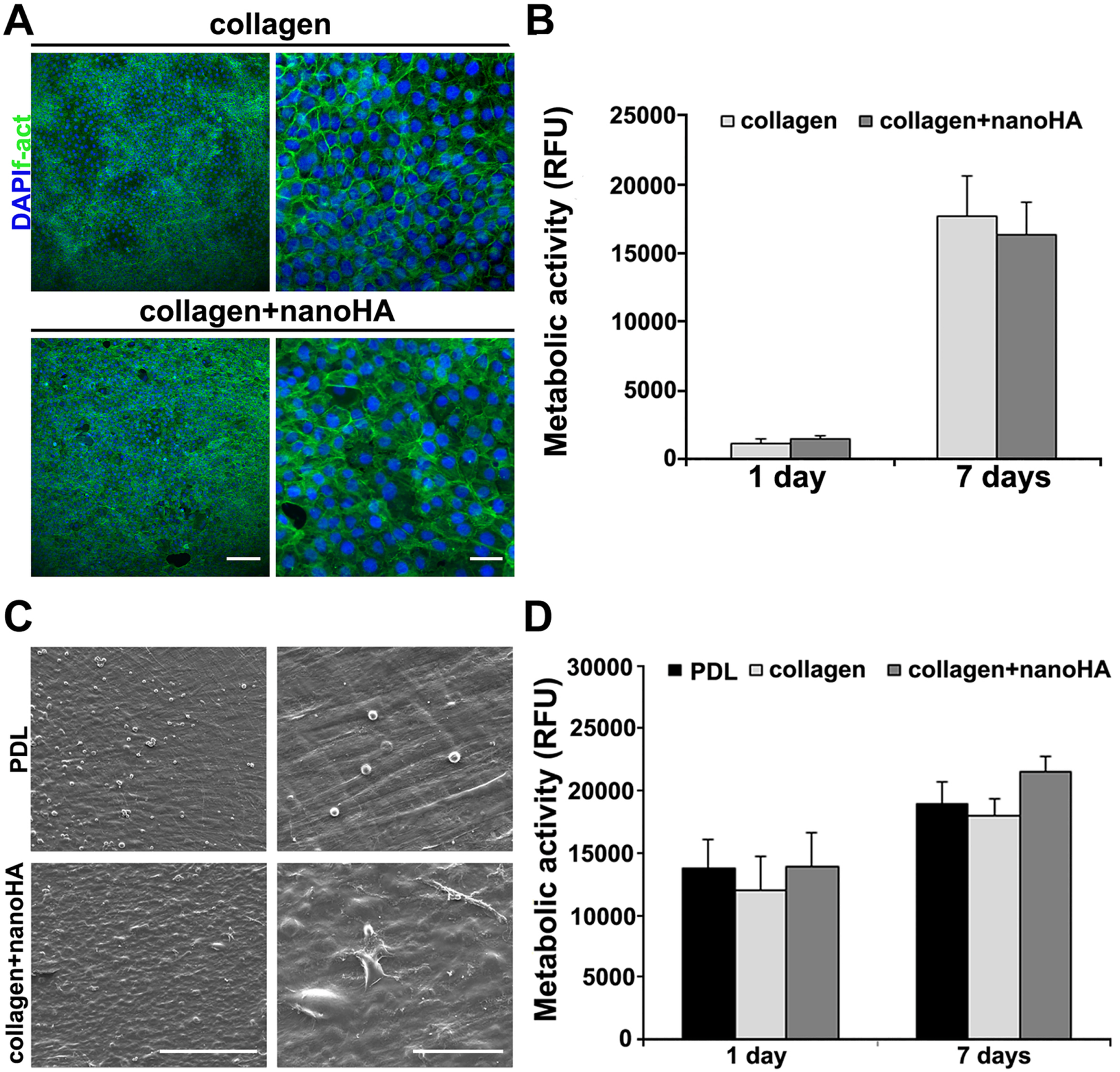
A
collagen
DAPI f-act
collagen+nanoHA
B
Metabolic activity (RFU)
25000
20000
15000
10000
5000
0
collagen
collagen+nanoHA
1 day
7 days
C
PDL
collagen+nanoHA
D
Metabolic activity (RFU)
30000
25000
20000
15000
10000
5000
0
PDL
collagen
collagen+nanoHA
1 day
7 days

Figure 4

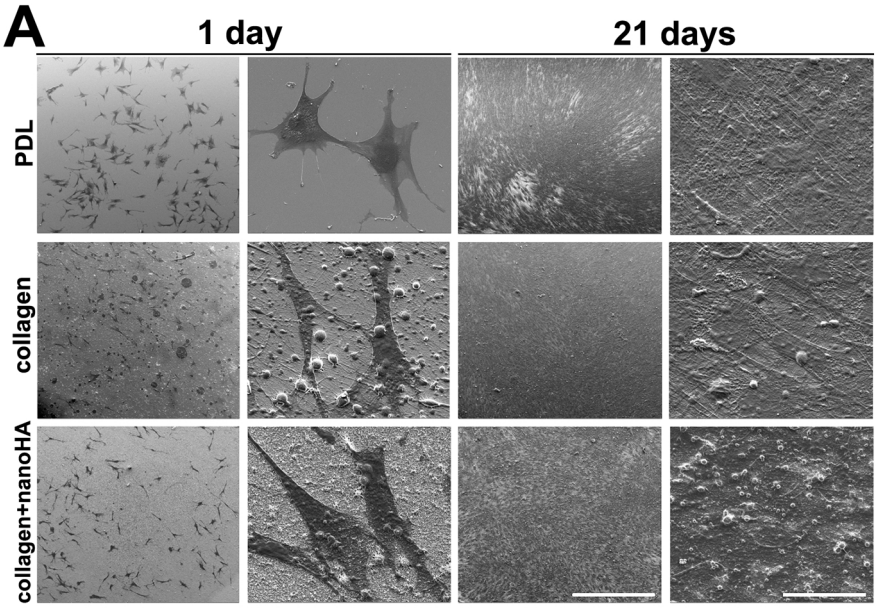
A
1 day
21 days
PDL
collagen
collagen+nanoHA

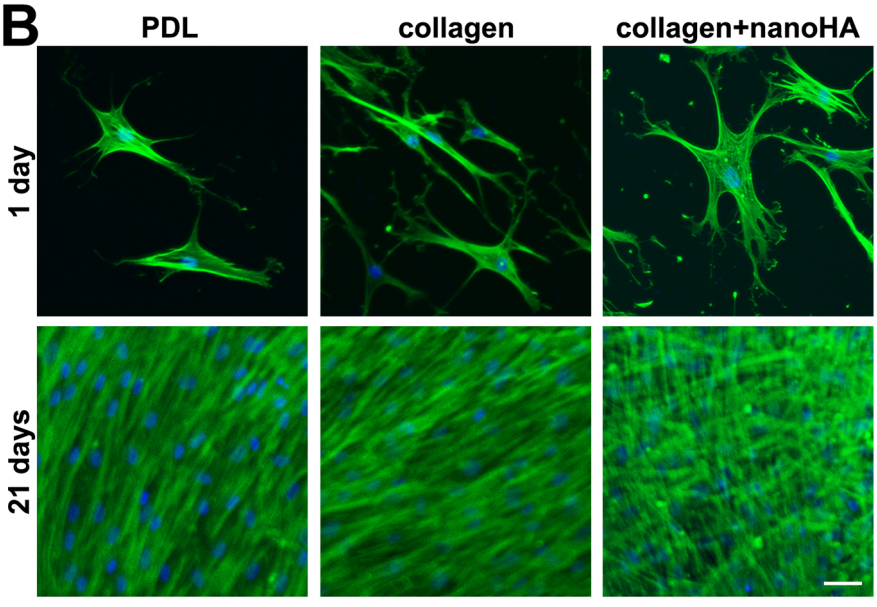
B
PDL
collagen
collagen+nanoHA
1 day
21 days

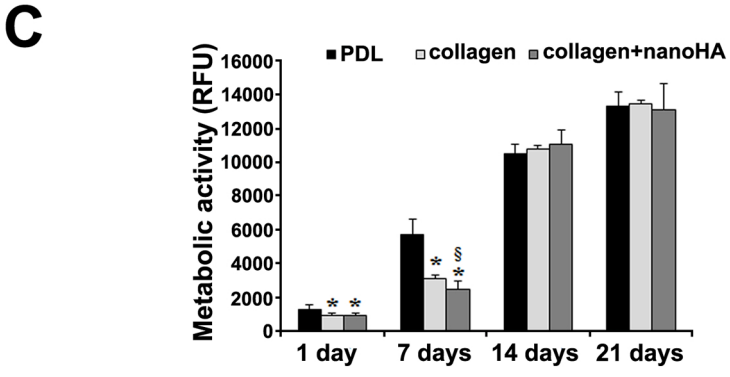
C
PDL
collagen
collagen+nanoHA
Metabolic activity (RFU)
16000
14000
12000
10000
8000
6000
4000
2000
0
*
*
*
§
1 day
7 days
14 days
21 days

Figure 5

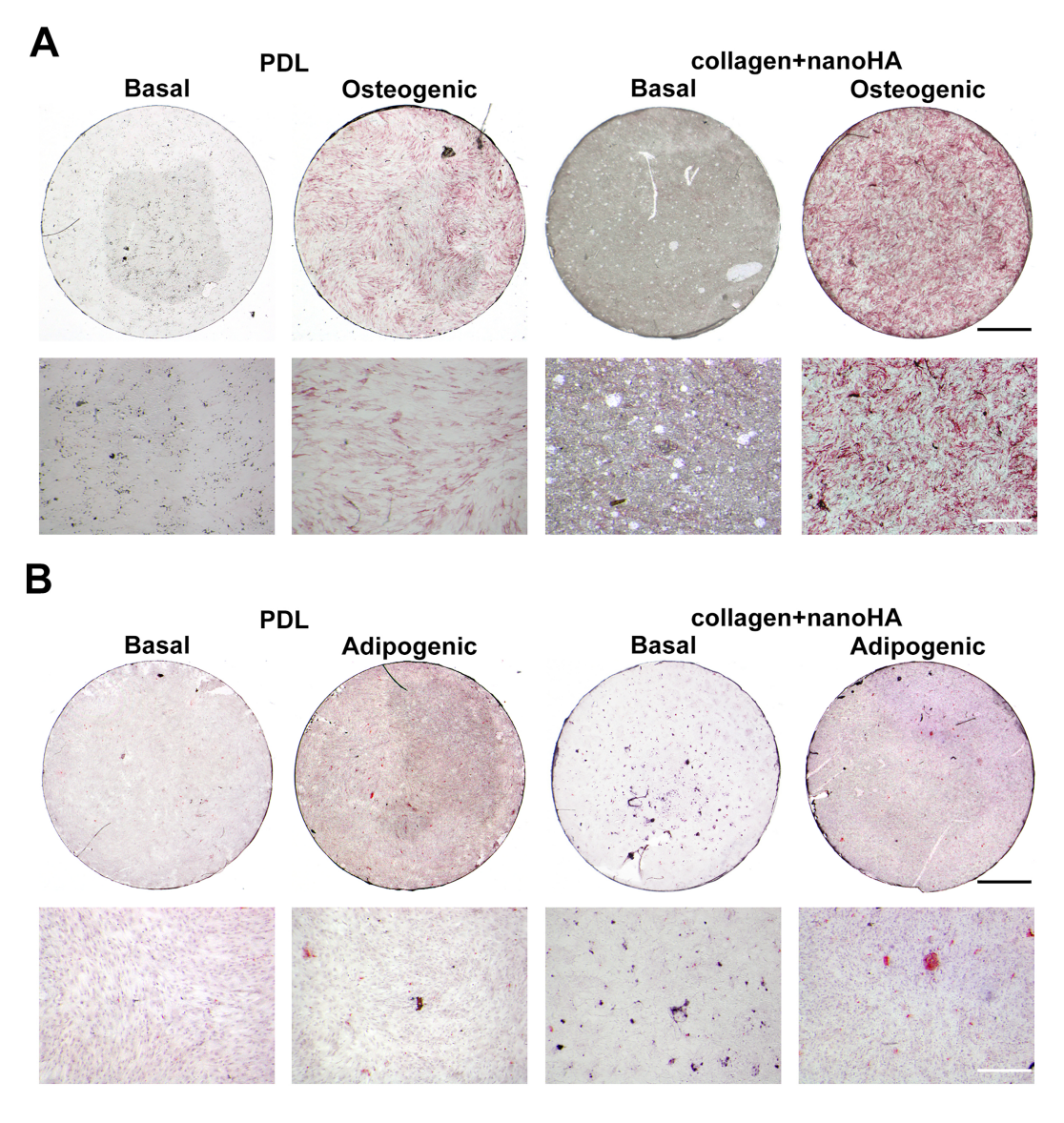
A
PDL
collagen+nanoHA
Basal
Osteogenic
Basal
Osteogenic
B
PDL
collagen+nanoHA
Basal
Adipogenic
Basal
Adipogenic

Figure 6

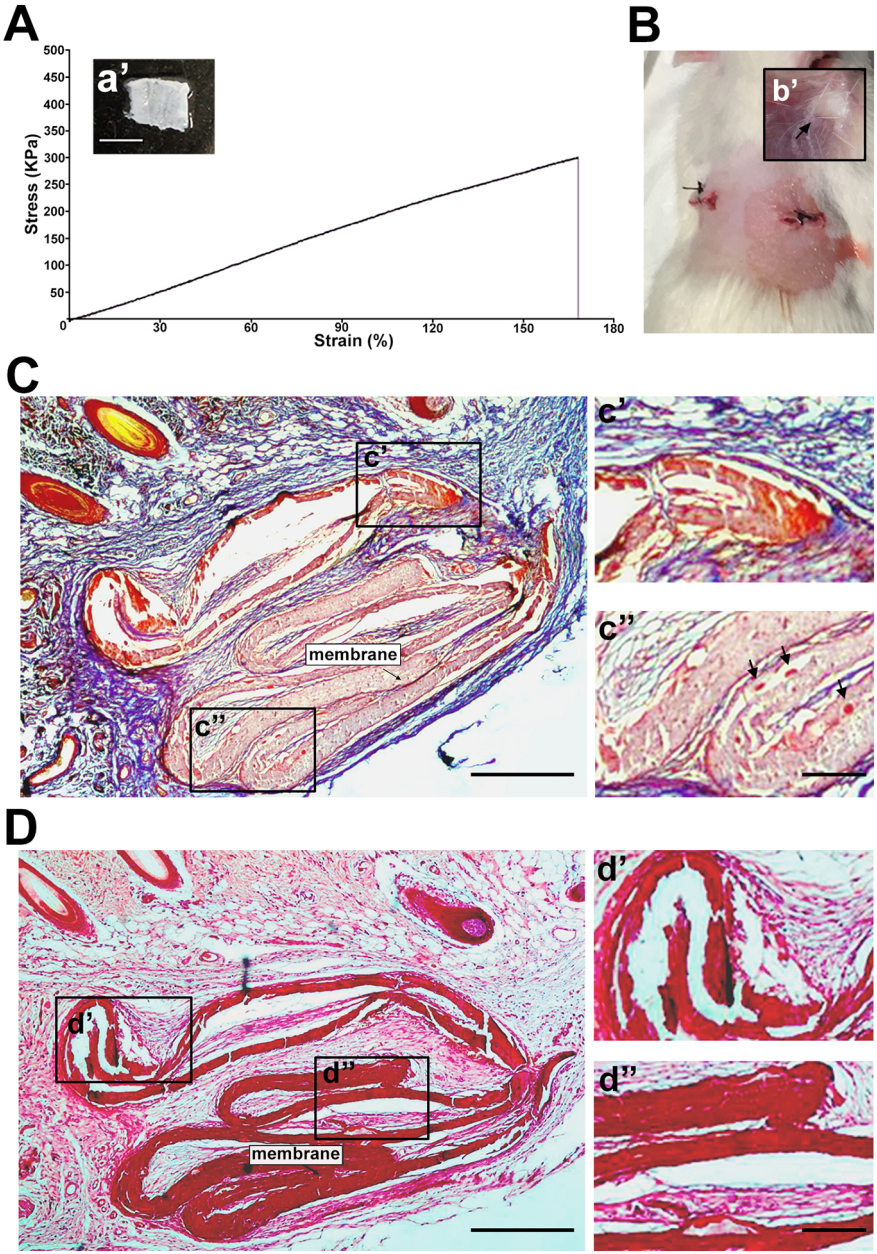
A
a'
Stress (KPa)
500
450
400
350
300
250
200
150
100
50
0
30
60
90
120
150
180
Strain (%)
B
b'
C
c'
c''
membrane
c'
c''
D
d'
d''
membrane
d'
d''

Figure 7